Structural, electronic, vibrational, and dielectric properties of LaBGeO$_5$ from first principles

R. Shaltaf,[1,a)] H. K. Juwhari,[1] B. Hamad,[1] J. Khalifeh,[1] G.-M. Rignanese,[2,3] and X. Gonze[2,3]

[1]*Department of Physics, The University of Jordan, 11942 Amman, Jordan*
[2]*Institute of Condensed Matter and Nanosciences (IMCN/NAPS), Université Catholique de Louvain (UCL),*
8 Chemin des étoiles, B-1348 Louvain-la Neuve, Belgium
[3]*European Theoretical Spectroscopy Facility (ETSF)*

Structural, electronic, vibrational, and dielectric properties of LaBGeO$_5$ with the stillwellite structure are determined based on *ab initio* density functional theory. The theoretically relaxed structure is found to agree well with the existing experimental data with a deviation of less than 0.2%. Both the density of states and the electronic band structure are calculated, showing five distinct groups of valence bands. Furthermore, the Born effective charge, the dielectric permittivity tensors, and the vibrational frequencies at the center of the Brillouin zone are all obtained. Compared to existing model calculations, the vibrational frequencies are found in much better agreement with the published experimental infrared and Raman data, with absolute and relative rms values of 6.04 cm^{-1}, and 1.81%, respectively. Consequently, numerical values for both the parallel and perpendicular components of the permittivity tensor are established as 3.55 and 3.71 (10.34 and 12.28), respectively, for the high-(low-)frequency limit. © *2014 AIP Publishing LLC.*
[http://dx.doi.org/10.1063/1.4866357]

I. INTRODUCTION

Natural stillwellite[1,2] is a rare earth mineral, which accepts a very wide range of substitutions, described by the general formula (Ln^{+3}, M^{+2})B(Si, Ge, Al, P)(O, OH, F)$_{5.0}$ where $Ln =$ La, Ce, Pr, or Nd. Among these, LaBGeO$_5$ (LBG) can be taken as a prototype to represent the series of the larger rare-earth borogermanate stillwellite compounds. LBG is well-known for its fascinating ferroelectric and non-linear optical properties.[3,4]

LBG is characterized by its low ferroelectric transition temperature, Tc = 530 C. It exhibits a significant pyroelectric coefficient ~5–10 nC cm^{-2} K^{-1}, a low dielectric constant (~11), a dielectric loss of (tan$\delta \sim 0.001$) at room temperature, a second harmonic generation efficiency (SHG) of ~30 units of α quartz. It also maintains a high electric resistance up to ~500 °C.[5–8] Due to these appealing interesting properties, LBG has drawn considerable interest in recent years. Some of its applications are a self-doubling laser;[9,10] and more recently, a substrate for growing high-quality crystalline InN thin films.[11]

The LBG crystal has a trigonal stillwellite (CeBSiO$_5$)-type structure, with a P_{31} space group symmetry and three formula units (Z = 3) per unit cell (Fig. 1). The principal structural units of stillwellite consist of infinite helical chains of BO$_4$ tetrahedra running parallel to the threefold screw axis, with each three tetrahedra forming a ring. Meanwhile, the GeO$_4$ tetrahedra were found to be connected to the remaining free vertices of one adjacent boron tetrahedron and to the lanthanide polyhedra.

Several groups have studied the polarized and unpolarized infrared (IR) and Raman spectra of LBG.[12–15] Hrubá *et al.*[15] carried out an investigation of the Infrared (IR) and Raman inelastic scattering in the temperature range of 300 to 870 K. They reported the vibrational frequencies and the frequency-dependent dielectric function. On the other hand, based on a short-range potential functional calculation model, Smirnov *et al.*[16] reported the IR and Raman spectral active modes of LBG.

In the present study, we extend such previous results, and present detailed calculations of the vibrational and dielectric properties of LBG using the state of the art *ab initio* density functional and density functional perturbation theories. The agreement between the experimental reflectivity and our computed reflectivity, shown in Fig. 3, is excellent. To the best of our knowledge, there had been no previous first-principle study of LBG properties, be they electronic or vibrational.

After the present introductory section, we detail our method of calculation (Sec. II), and we present our results (Sec. III), concerning respectively the structural properties, the electronic properties, the Born effective charge, the vibrational and dielectric properties. We then conclude (Sec. IV).

II. METHOD OF CALCULATIONS

The calculations have been performed using the state of the art *ab initio* plane-wave density functional method, as implemented in the ABINIT code.[17] The all-electron potential is approximated by norm-conserving pseudopotentials generated within the Troullier-Martin[18] and extended Teter schemes.[19] The pseudopotentials are constructed considering the following states as valence states: La($5s^2$, $5p^6$, $6s^2$, $5d^1$), Ge($3s^2$, $3p^6$), B($3s^2$, $3p^1$), and O($2s^2$, $2p^4$). The wave functions are expanded into a plane-wave basis set up to a kinetic energy cutoff of 40 Ha. The Brillouin zone integration is performed using a special $4 \times 4 \times 4$ grid of k-points generated with the Monkhorst-Pack scheme.[20] We have checked that

a)E-mail: r.shaltaf@ju.edu.jo
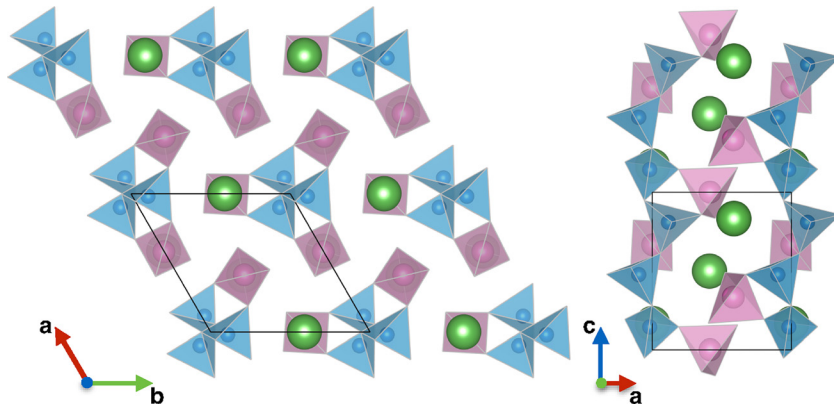
FIG. 1. Schematic representation of the LaBGeO$_5$ stillwellite crystalline structure: top (left panel) and side (right panel) views. La atoms are in green, Ge tetrahedra in pink, and B tetrahedra in blue.

the computations are well converged with these numerical parameters. The density of states calculations are carried out using the tetrahedron method using a $16 \times 16 \times 16$ grid of k-points. The electron-electron interaction is approximated within local-density approximation (LDA).[21] Relaxations of the lattice parameters and internal atomic positions within the unit cell were performed using the BFGS algorithm[22] until the maximum component of the force acting on any atoms has dropped below 10^{-6} Hartree/Bohr and until the maximal stress is lower than 10^{-5} Hartree/Bohr^3. Linear-response calculations, yielding vibrational, and dielectric properties are performed using density functional perturbation theory.[23]

III. RESULTS

A. Structural properties

The calculated atomic positions (this work) of the non-equivalent atoms (one unit) are shown in Table I along with the existing experimental results. The structural parameters of the other atoms in the unit cell can still be calculated by invoking symmetry operations. The calculated lattice parameters gave values of $a = 6.957$ Å and $c = 6.742$ Å. These results are in good agreement compared with the reported experimental X-ray single-crystal diffraction values of $a = 7.002$ Å and $c = 6.860$ Å (Ref. 24) and with the high-resolution neutron powder diffraction values of $a = 7.0018$ Å and $c = 6.8606$ Å.[8] The theoretical results that have been predicted by this investigation underestimate the experimental lattice parameters by less than 2%, which is a typical LDA error. Table II shows the inter-atomic distances of anion-

oxygen for B and Ge tetrahedra as well as La Polyhedra. Both B and Ge tetrahedra are connected to O1 and O2. The Ge-O1(O2) are almost the same. A similar behavior is found in the case of B-O1(O2). The atoms O3 and O4 represent free vertex of the Ge tetrahedra with distances slightly smaller than those of Ge-O1(O2). The atom O5 is a bridge connecting adjacent B tetrahedra. Similar to the case of Ge, the B-O5s distances are found slightly smaller than those of B-O1(O2). The result makes it easier to distinguish between three different classes of oxygen atoms according to their environment. The first class consists of O1 and O2, the second consists of O3 and O4, and the last class is represented by O5 atoms. The relaxed ionic structure at fixed lattice parameters was also calculated and the results are presented in Tables I and II. In this investigation, it was found that relaxing the ionic position at fixed experimental lattice parameter is a better choice than considering the shorter LDA lattice parameters to obtain a vibrational structure in agreement with experimental data.

B. Electronic properties

The electronic density of states accompanied by the electronic band structure along the high symmetry lines[25] have been computed as shown in Figure 2. We found that the minimum gap is indirect at Γ-K with a value of 4.54 eV. The minimum direct gap has almost the same value and exists at Γ. However, it is a well-known fact that the Density Functional Theory (DFT) predictions underestimate the value of the electronic gap. For similar materials, an underestimation by 2 eV is not uncommon. A more precise value of the gap can be

TABLE I. Comparison of the calculated internal atomic parameters with the experimental results from Ref. 24. The results in italic are theoretical results obtained when fixing the lattice constants at their experimental values.

	Theory						Experiment		
	x/a		y/a		z/c		x/a	y/a	z/c
La	0.4127	*0.4120*	−0.0009	*−0.0009*	0.3346	*0.3378*	0.4107	−0.0007	0.333
B	−0.1613	*−0.1145*	−0.0158	*−0.0143*	0.3069	*0.3111*	−0.114	−0.010	0.313
Ge	0.4191	*0.4171*	0.0064	*−0.0041*	0.8362	*0.8384*	0.4200	−0.0033	0.834
O1	0.1545	*0.1538*	0.3495	*0.3474*	0.0179	*0.0201*	0.1538	0.3438	0.0116
O2	0.3275	*0.3279*	0.1415	*0.1414*	0.9924	*0.9923*	0.3320	0.1450	0.9912
O3	0.1347	*0.1337*	0.6101	*0.6082*	0.3385	*0.3402*	0.1440	0.6125	0.3349
O4	0.6063	*0.6062*	0.1570	*0.1522*	−0.3384	*−0.3334*	0.6081	0.153	−0.3341
O5	0.0153	*0.0119*	0.0625	*0.0579*	0.7731	*0.7807*	0.0131	0.057	0.7807

TABLE II. Anion-oxygen interatomic distances (in Å). Prime indices refer to equivalent atoms in the same or adjacent unit cells.
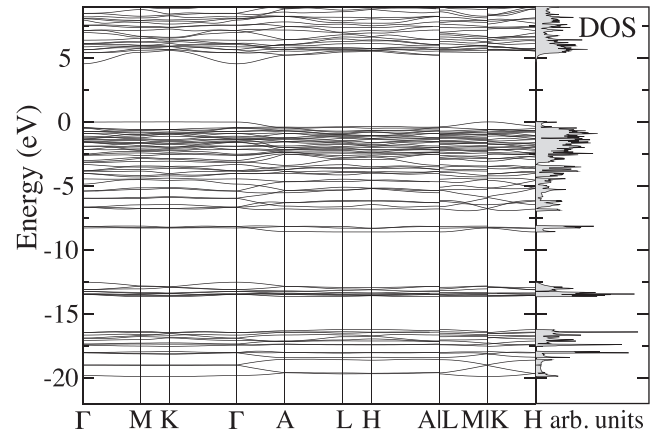
	La polyhedra		Ge tetrahedra	B tetrahedra
Theory @ $V_{Th.}$	O1: 2.719	O1′: 2.606	O1: 1.730	O1: 1.501
	O2: 2.692	O2′: 2.699	O2: 1.732	O2: 1.506
	O3: 2.415	O3′: 2.530	O3: 1.673	O5: 1.448
	O4: 2.414	O4′: 2.530	O4: 1.678	O5′: 1.446
	O5: 2.594			
Theory @ $V_{Expt.}$	O1: 2.753	O1′: 2.634	O1: 1.739	O1: 1.507
	O2: 2.747	O2′: 2.721	O2: 1.740	O2: 1.513
	O3: 2.435	O3′: 2.574	O3: 1.682	O5: 1.457
	O4: 2.435	O4′: 2.575	O4: 1.686	O5′: 1.455
	O5: 2.635			
Experiment	O1: 2.772	O1′: 2.651	O1: 1.782	O1: 1.488
	O2: 2.680	O2′: 2.684	O2: 1.772	O2: 1.535
	O3: 2.433	O3′: 2.566	O3: 1.625	O5: 1.414
	O4: 2.412	O4′: 2.589	O4: 1.761	O5′: 1.481
	O5: 2.672			

FIG. 2. Electronic band structure and density of states of LaBGeO$_5$. The Fermi level has been aligned to the top of the valence band.

obtained usually by employing many-body perturbation theory (the *GW* approximation), which is however beyond the scope of this study. However, although the DFT value of the electronic band gap is known to differ from the experimental one, the characteristics of the valence band are usually believed faithful.

As seen in Figure 2, five groups of bands are identified. The lowest set (not shown, consisting of 3 bands) is located at −28 eV, characterized by a sharp DOS peak, and attributed to La *s*-states. The second set (consisting of 15 bands), located between −20 and −16.5 and related to O *s*-bands, is slightly hybridized with Ge, B, and La orbitals. The third set (consisting of 9 bands) which is located between −13.5 and −12.5 eV, corresponds to La *p*−orbitals. The fourth bands (consisting of 3 bands) is located between −8.6 and −8.1 eV and attributed to B *s*-orbitals. This set is slightly hybridized with O *p*-orbitals. The last set, which has the largest dispersion (∼7 eV), is composed of a mix of O *p*-, La *d*-, and Ge *p*-, and B *p*-orbitals. The conduction band edge consists of a mix of La-*s*, La-*d*, and Ge-*s* with a slight hybridization of O orbitals. Analysis of the energy bands indicate a mixed ionic-covalent behavior, as will be confirmed in the following section.

C. Born effective charge

The Born effective charge tensor $Z^*_{\alpha\beta,j}$ is defined as the induced polarization of the solid along the Cartesian direction α by a unit displacement in the direction β of the sublattice generated by atom j. Equivalently, it is the force along the direction α on the atom j due to a homogeneous electric field in the direction β.[26] The effective charge tensors have been calculated for the eight non-equivalent atoms in the unit cell. The results are shown in Table III. The charge tensors for the remaining atoms of the unit cell can be still be obtained by invoking the symmetry operations. The charge neutrality sum rule ($\sum_j Z^*_{\alpha\beta,j} = 0$) is almost perfectly verified (with a total value lower than 0.05) suggesting that our results are well converged.

Since the local site symmetry of each ion in this structure *can be completely represented by* C_1, the charge tensors of all ions are anisotropic, with non-zero off-diagonal elements. Thus, it might be more convenient to analyze the charge tensor elements along the ion principal axis (the principal values).

The effective charge of each La-ion, between 3.73 and 4.61, is anomalously large compared to its nominal ionic charges (La: +3). This agrees well with what have been obtained in case of La$_2$O$_3$.[27] The anomalously large Z^* values indicate a strong dynamic charge transfer along the La-O bond, confirming the above-mentioned a mixed ionic–covalent bond.

TABLE III. Calculated Born effective charge tensors Z^* along with their principal values λ. The percentages indicate the relative deviations of the principal values from the isotropic values.

Ion	Z^*			λ		Ion	Z^*			λ	
La	3.82	0.06	−0.15	4.61	11%	Ge	3.18	−0.01	0.07	3.66	13%
	0.03	4.54	0.26	4.09	−1%		−0.04	2.92	−0.16	3.18	−2%
	−0.14	0.15	4.08	3.73	10%		0.02	−0.15	3.62	2.89	−11%
B	2.58	−0.14	0.12	2.83	11%	O1	−2.15	0.24	0.29	−2.57	30%
	−0.13	2.59	−0.14	2.44	−4%		0.33	−2.08	−0.26	−1.83	−8%
	0.17	−0.12	2.48	2.38	−7%		0.37	−0.15	−1.73	−1.55	−22%
O2	−2.10	−0.43	−0.18	−2.62	32%	O3	−1.27	−0.39	−0.07	−2.76	36%
	−0.53	−2.13	−0.07	−1.78	−11%		−0.37	−2.60	−0.14	−2.16	6%
	−0.20	0.01	−1.72	−1.55	−22%		−0.08	−0.17	−2.21	−1.17	−42%
O4	−1.28	0.36	0.06	−2.77	35%	O5	−1.44	0.39	−0.03	−2.74	45%
	0.37	−2.63	−0.10	−2.19	7%		0.35	−1.95	−0.58	−1.78	−6%
	0.07	−0.17	−2.23	−1.19	−42%		−0.02	0.54	−2.29	−1.16	−39%

TABLE IV. Calculated and experimental TO and LO frequencies (in cm^{-1}). The contributions of the phonon modes to the static dielectric tensor $\Delta\varepsilon$ are indicated.

Mode	DFPT at $V_{\text{Expt.}}$			DFPT at $V_{\text{Th.}}$			Model (Ref. 16)		Experiment (Ref. 15)		
	TO	LO	$\Delta\varepsilon$	TO	LO	$\Delta\varepsilon$	TO	$\Delta\varepsilon$	TO	LO	$\Delta\varepsilon$
E_1	90	90	0.05	89	89	0.04	101	1.07	92	93	0.27
E_2	110	111	0.13	113	114	0.12	119	1.43	109	110	0.29
E_3	128	128	0.15	133	133	0.01	125	1.85	124	125	0.34
E_4	163	176	2.86	162	180	2.47	141	0.22	162	179	2.99
E_5	183	197	0.56	196	199	0.42	187	0.05	187	200	0.48
E_6	207	211	0.11	214	214	0.17	214	0.00	207	208	0.05
E_7	221	222	0.04	234	235	0.04	245	0.01	233	234	0.08
E_8	259	261	0.14	263	265	0.14	289	0.09	258	262	0.22
E_9	307	321	0.90	310	324	0.81	319	0.57	301	320	1.00
E_{10}	333	347	0.29	345	363	0.44	370	0.14	336	352	0.29
E_{11}	377	391	0.31	390	402	0.23	382	0.21	384	396	0.23
E_{12}	418	431	0.17	431	446	0.19	456	0.01	423	439	0.20
E_{13}	446	446	0.00	458	460	0.01	518	0.00	(454)		…
E_{14}	485	489	0.06	500	503	0.05	557	0.01	496	502	0.08
E_{15}	609	611	0.05	624	626	0.04	653	0.00	616	621	0.11
E_{16}	690	690	0.02	702	703	0.04	719	0.03	695	701	0.32
E_{17}	723	743	0.32	737	756	0.33	717	0.03	722	753	0.33
E_{18}	790	824	0.37	811	847	0.38	785	0.04	784	811	0.19
E_{19}	835	843	0.02	859	866	0.02	809	0.02	826	834	0.02
E_{20}	869	872	0.02	892	895	0.01	861	0.04	859	863	0.02
E_{21}	912	923	0.10	930	943	0.10	936	0.04	918	928	0.08
E_{22}	971	1031	0.25	998	1056	0.24	968	0.01	975	1042	0.30
E_{23}	1092	1095	0.00	1120	1124	0.01	1043	0.03	1088	1098	0.01
A_1	91	93	0.47	90	90	0.00	105	0.10	87	89	0.46
A_2	97	97	0.02	95	96	0.31	110	0.16	95	96	0.02
A_3	118	122	1.15	124	126	0.60	122	0.45	117	119	0.63
A_4	148	149	0.18	154	155	0.17	142	0.07	144	145	0.21
A_5	166	184	4.46	186	196	3.34	163	1.31	173	213	4.28
A_6	184	210	0.00	199	212	0.07	…	…	…	…	…
A_7	210	217	0.01	213	230	0.04	198	0.01	215	222	0.01
A_8	280	280	0.00	283	283	0.00	284	0.00	(273)		…
A_9	301	302	0.04	306	307	0.04	304	0.02	(301)		…
A_{10}	303	304	0.01	319	319	0.00	340	0.25	306	307	0.05
A_{11}	322	327	0.23	334	334	0.19	375	0.00	324	329	0.26
A_{12}	372	381	0.68	381	395	0.82	401	0.47	368	380	0.76
A_{13}	388	419	0.34	403	433	0.29	485	0.00	389	422	0.34
A_{14}	492	501	0.14	498	509	0.15	555	0.00	503	510	0.11
A_{15}	539	544	0.07	550	556	0.07	599	0.00	546	552	0.03
A_{16}	624	626	0.03	637	640	0.03	697	0.00	631	633	0.03
A_{17}	732	744	0.20	749	762	0.18	752	0.04	733	745	0.20
A_{18}	810	817	0.12	830	836	0.08	792	0.00	799	803	0.12
A_{19}	818	819	0.00	840	840	0.00	800	0.16	806	813	0.04
A_{20}	850	854	0.09	870	872	0.08	…	…	847	852	…
A_{21}	860	873	0.11	880	896	0.13	848	0.01	864	866	0.04
A_{22}	948	981	0.43	986	1005	0.34	930	0.01	941	980	0.51
A_{23}	990	1043	0.07	1013	1074	0.10	1034	0.07	992	1050	0.08

For Ge and B ions, the effective charges are noticeably smaller than their nominal ionic charges (Ge: +4, B: +3). The presence of five non-equivalent oxygen atoms is reflected in differences between their Born effective charge tensors. Hence, 3 different types of Oxygen atoms are recognized, where O1 and O2 is each connected to Ge and B tetrahedra simultaneously. O5 is a bridge between two B tetrahedra. O3 and O4 are each connected to a single Ge atom.

The anisotropy of the effective charge tensor is measured by considering the deviation of each principal value from the isotropic value. The anisotropy of La-ion charge tensor is found to be (11, −1, and −10%). In case of Ge (13, −2, −11%), and (11, −4, −7%) for B. The weak anisotropy of La-, Ge-, B-ions can be understood in terms of the bonding environment. Each La-ion is surrounded by 9 O-ions with close bonding lengths.

TABLE V. The dielectric permittivity tensor components along and perpendicular to the trigonal axis. The sums of ionic contributions to static dielectric tensor $\Delta\varepsilon_{tot}$ are also indicated.

	$\varepsilon_{\parallel}$	$\varepsilon_{\perp}$
ε_{∞}	3.55	3.71
$\Delta\varepsilon_{tot}$	6.79	8.57
ε_0	10.34	12.28

Similar arguments can be drawn for Ge and B where both are connected by tetrahedral bonds to O-ions. Despite the small differences in bond lengths, still the isotropic environment remains a valid scenario.

D. Vibrational and dielectric properties

Group theory analysis, for space group C_3, indicates that the irreducible representations of phonon modes at Γ are

$$\Gamma_{vib} = 24E \oplus 24A,$$

where E and A modes are doubly and singly degenerate modes, respectively, and generate together a total of 72 modes. The E modes are marked by collective displacement patterns in the $x - y$ plane, while the A modes has collective displacements along the z direction. Due to absence of the center of inversion, all modes allow simultaneous IR and Raman activities. The contribution of these modes to the frequency dependent dielectric permittivity is calculated via

$$\varepsilon_{\alpha\beta}^0(\omega) = \varepsilon_{\alpha\beta}^\infty + \sum_m \Delta\varepsilon_{\alpha\beta,m}(\omega),$$

where $\Delta\varepsilon_{\alpha\beta,m}$ is the contribution of the vibrational mode m to the dielectric tensor along the Cartesian coordinates α and β and given as

$$\Delta\varepsilon_{\alpha\beta,m}(\omega) = \frac{4\pi}{V} \frac{S_{\alpha\beta,m}}{\omega_m^2 - \omega^2 - i\Omega\omega}.$$

$S_{\alpha\beta,m}$ is the mth mode oscillator strength along both α and β direction. The damping frequency Ω is taken to be identical for all modes with a value $7\,cm^{-1}$.

The infrared reflectivity is related to the frequency dependent dielectric permittivity as

$$R(\omega) = \left| \frac{\sqrt{\varepsilon_{\alpha\beta}^0(\omega)} - 1}{\sqrt{\varepsilon_{\alpha\beta}^0(\omega)} + 1} \right|^2.$$

The calculated phonon frequencies at the center of the Brillouin zone Γ, computed in this work, are compared with measured values and presented in Table IV. For comparison reasons, phonon frequencies from theoretical model calculations are also cited. For each mode, longitudinal and transverse optical (LO) and (TO) frequencies are being shown. Such splitting is normally attributed to the long range dipole-dipole interaction. Results from this investigation demonstrate good agreement with existing experimental data with

absolute and relative rms values of $6.04\,cm^{-1}$ and 1.81%, respectively.

Two additional A modes are found at $184\,cm^{-1}$ and $301\,cm^{-1}$, respectively. They are marked by their low oscillator strengths and as such introduce a negligible contributions to the dielectric permittivity, which explains why they were not detected experimentally.

Due to the trigonal symmetry of the crystal, the electronic ε_{∞} and static dielectric tensors ε_0 possess two independent components $\varepsilon_{\parallel}$ and $\varepsilon_{\perp}$, along and perpendicular to the c axis, respectively.

These values of ε_{∞} and ε_0 are presented in Table V. It has been noticed that the major mode contribution to $\varepsilon_{\perp}$ comes from E_4 mode (experimentally observed at $163\,cm^{-1}$), with $\Delta\varepsilon = 2.77$, that is nearly 40% of the overall lattice contribution. This outcome agrees reasonably well with the experimental findings that $\Delta\varepsilon$ of the equivalent mode is found to be the largest among other modes, with a value around 2.99. Similar agreement has been found in the case of $\varepsilon_{\parallel}$, the largest ionic contribution coming from the A_5 mode (experimentally observed at $173\,cm^{-1}$), with $\Delta\varepsilon = 4.33$ in reasonable agreement with the experimental value of 4.28. The large contribution from these modes, found experimentally, had not been reproduced by the model calculations of Ref. 16. Analyzing the eigen displacement of the modes with the highest $\Delta\varepsilon$, namely, E_4 and A_5, we found that these modes are characterized by rigid unit translations of Ge and B tetrahedra opposite to La ions.

In general, we found that the low-frequency modes have significant contributions to the dielectric tensor due to the large displacement of the La ions (for which the Born effective charge is anomalously large, as mentioned in the previous section). This is in contrast with high-frequency modes which have less contribution to the dielectric tensor, due to negligible displacements of the La ions.

The calculated IR reflectivity and dielectric loss are presented in Figs. 3 and 4, respectively, along with the correspondent measured data. The overall agreement between both calculated and experimental results is rather good as all the major features of the experimental infrared spectra are already obtained.

For comparison reasons, it is noted that ε_{∞} can be estimated from the refraction index n, which has been reported
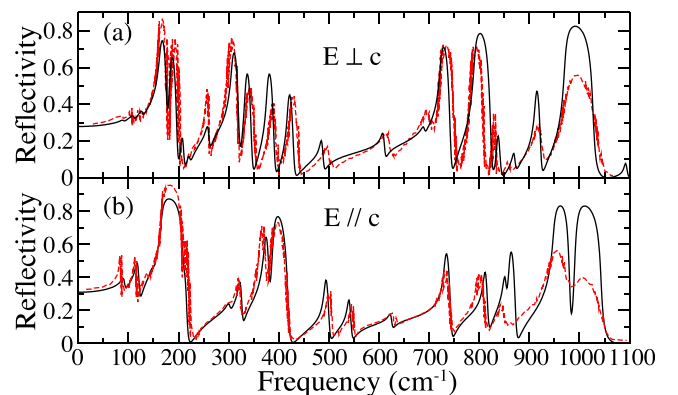

FIG. 3. Calculated (black) and measured (red) IR reflectivity parallel and perpendicular to the trigonal axis. The experimental results are from Ref. 15.
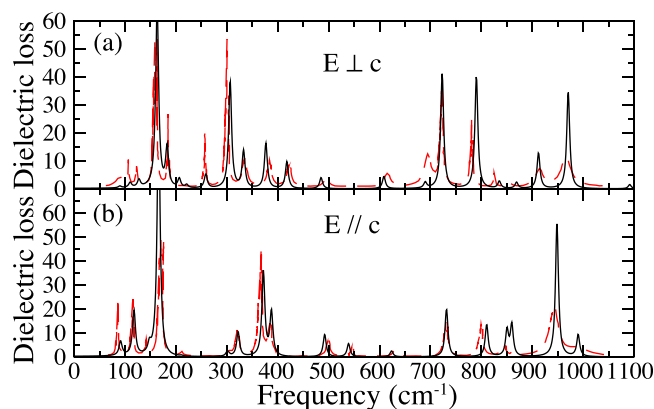
FIG. 4. Calculated (black) and measured (red) dielectric loss parallel and perpendicular to the trigonal axis. The experimental results are from Ref. 15.

experimentally to be about 1.88,[13] $\varepsilon_\infty = n^2 = 3.53$. The calculated values of ε_∞ are 3.55 and 3.71 for the perpendicular and parallel components, respectively. The anisotropy is weak, although non-negligible. They are in excellent agreement with experimental measurements.

In fact, the reported value of $\varepsilon_0 = 11$ falls nicely between the presently calculated values of 10.34 and 12.28 for the perpendicular and parallel components, respectively. The ionic contribution to ε_0 is much more anisotropic than the electronic contribution.

Our results suggest potential applications for flat panel displays. This field is expanding very quickly and will soon turn into a multibillion dollar market, driven by the wide usage of mobile devices and public display systems. New multipurpose smart materials are actively sought in this framework. The stillwellite family, including $LaBGeO_5$, is considered a potential phosphor host as it can accept a wide range of substitutions including all rare-earth ions while still maintaining its brilliant dielectric properties.[28,29]

The calculated values of the perpendicular and parallel components of dielectric constants are found to be close, on average, to those of ($PbO-SiO2-B2O3-Nd2O3$) previously proposed to be used for plasma display panels.[30] Moreover, the slight difference in the magnitudes of the two components of ε_0 will likely impose no restriction on the various deposition techniques that might be employed during the preparation processes, if used in the flat panel displays.

IV. CONCLUSION

A comprehensive study of the structural, electronic, vibrational, and dielectric properties of the $LaBGeO_5$ compound with the stillwellite structure has been presented in this investigation using *ab initio* density functional theory. The structural parameters of this compound were found to agree well with the available experimental data with a negligible deviation of less than 0.2%. The DFT electronic structure, which had not yet been computed, has been presented. The calculated vibrational and dielectric properties of this representative compound of the larger rare-earth borogermanate family of the stillwellite structure are found to fit neatly

and therefore consolidate the existing experimental published results. In particular, we improve the agreement significantly with respect to the previous model calculation. As a future work, it would be of great interest to investigate the effect of rare earth dopants on the electronic, dielectric, and optical properties of $LaBGeO_5$ for potential use as phosphors in flat panel displays.

[1] J. McAndrew and T. R. Scott, Nature **176**, 509 (1955).
[2] H. K. Juwhari and W. B. White, Mater. Lett. **64**, 1751 (2010).
[3] D. Vouagner *et al.*, Philos. Mag. **87**, 535 (2007).
[4] D. Vouagner *et al.*, J. Non-Cryst. Solids **353**, 1910 (2007).
[5] S. Yu. Stefanovich, B. V. Mill, and A. V. Butashin, Kristallografiya **37**, 965 (1992) [Sov. Phys. Crystallogr. **37**, 513 (1992)].
[6] A. Onodera *et al.*, J. Phys. Soc. Jpn. **62**, 4311 (1993).
[7] V. N. Sigaev *et al.*, J. Non-Cryst Solids **353**, 1956 (2007).
[8] E. L. Belokoneva, W. I. F. David, J. B. Forsyth, and K. S. Knight, J. Phys.: Condens. Matter **9**, 3503 (1997).
[9] J. Capmany, D. Jaque, J. García Solé, and A. A. Kaminskii, Appl. Phys. Lett. **72**, 531 (1998).
[10] J. Capmany and J. García Solé, Appl. Phys. Lett. **70**, 2517 (1997).
[11] S. Miyazawa *et al.*, Phys. Status Solidi A **208**, 1195–1198 (2011).
[12] A. Rulmont and P. Tarte, Solid State Chem. **75**, 244 (1988).
[13] A. A. Kaminskii *et al.*, Phys. Status Solidi A **125**, 671 (1991).
[14] R. V. Pisarev and M. Serhane, Phys. Solid State **37**, 2022 (1995).
[15] I. Hrubá *et al.*, Phys. Status Solidi B **214**, 423 (1999).
[16] M. B. Smirnov, A. V. Menschikova, I. Kratochvilova-Hruba, and Z. Zikmund, Phys. Status Solidi B **241**, 1017 (2004).
[17] X. Gonze *et al.*, Comput. Phys. Commun. **180**, 2582 (2009).
[18] N. Troullier and J. L. Martins, Phys. Rev. B **43**, 1993 (1991).
[19] M. P. Teter, Phys. Rev. B **48**, 5031 (1993).
[20] H. J. Monkhorst and J. D. Pack, Phys. Rev. B **13**, 5188 (1976).
[21] J. P. Perdew and Y. Wang, Phys. Rev. B **45**, 13244 (1992).
[22] W. H. Press, B. P. Flannery, S. A. Teukolsky, and W. T. Vetterling, *Numerical Recipes: The Art of Scientific Computing, FORTRAN Version*, (Cambridge University Press, Cambridge, 1989).
[23] S. Baroni, S. de Gironcoli, A. Dal Corso, and P. Giannozzi, Rev. Mod. Phys. **73**, 515 (2001).
[24] E. L. Belokoneva, B. V. Mill, A. V. Butashin, and A. A. Kaminskii, Izv. Akad. Nauk SSSR, Ser. Neorg. Mater. **27**, 556 (1991).
[25] W. Setyawan and S. Curtarolo, Comput. Mater. Sci. **49**, 299 (2010).
[26] Ph. Ghosez, J.-P. Michenaud, and X. Gonze, Phys. Rev. B **58**, 6224 (1998).
[27] R. Vali and S. M. Hosseini, Comput. Mater. Sci. **31**, 125 (2004).
[28] H. Zou, X. Hui, X. Wang, D. Peng, J. Li, Y. Li, and X. Yao, J. Appl. Phys. **114**, 223103 (2013).
[29] S. Zhang, G. Wu, C. Duan, and J. Wang, J. Rare Earth **29**, 737 (2011).
[30] D. K. Lee, Y. Cho, S. H. Sohn, and H. K. Kim, J. Korean Phys. Soc. **45**, 1236 (2004).